UCRL-51682, Pt. 6

BEHAVIOR OF POROUS BERYLLIUM UNDER THERMOMECHANICAL LOADING

PART 6: EFFECT OF PRESSURE ON THE MICROSTRUCTURE OF PLASMA-SPRAYED BERYLLIUM

J. E. Hanafee
E. O. Snell

April 8, 1975

Prepared for U.S. Energy Research & Development Administration under contract No. W-7405-Eng-48

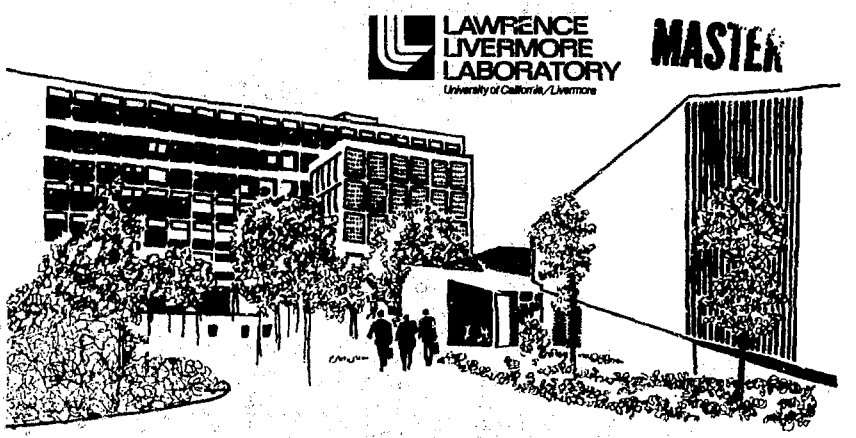

Printed in the United States of America
Available from
National Technical Information Service
U. S. Department of Commerce
5285 Port Royal Road
Springfield, Virginia 22151
Price: Printed Copy $___*; Microfiche $2.25

*Pages	NTIS Selling Price
1-50	$4.00
51-150	$5.45
151-325	$7.60
326-500	$10.60
501-1000	$13.60

Distribution Category
UC-34

LAWRENCE LIVERMORE LABORATORY
University of California/Livermore, California/94550

UCRL-51682, Pt. 6

BEHAVIOR OF POROUS BERYLLIUM UNDER THERMOMECHANICAL LOADING

PART 6: EFFECT OF PRESSURE ON THE MICROSTRUCTURE OF PLASMA-SPRAYED BERYLLIUM

J. E. Hanafee
E. O. Snell

MS. date: April 8, 1975

Preface

This report is Part 6 of a seven-part series on Behavior of Porous Beryllium Under Thermomechanical Loading (UCRL-51682 Pts. 1-7). The titles and authors of the individual reports in the series are as follows:

Title	Author
Part 1. Summary of Results	W. M. Isbell
Part 2. Quasi-Static Deformation	R. N. Schock, A. E. Abey, and A. G. Duba
Part 3. Shock Wave Studies	W. M. Isbell and R. R. Horning
Part 4. Constitutive Model for Wave propagation	F. H. Ree, W. M. Isbell, and R. R. Horning
Part 5. Electron-Beam Studies	O. R. Walton and W. M. Isbell
Part 6. Effect of Pressure on the Microstructure of Plasma-Sprayed Beryllium	J. E. Hanafee and E. O. Snell
Part 7. Calibration Studies on the Carbon Piezoresistive Gage	R. R. Horning and W. M. Isbell

This work was supported by the Defense Nuclear Agency (Mr. Donald Kohler, technical monitor) under the auspices of the U. S. Energy Research & Development Administration.

Contents

BEHAVIOR OF POROUS BERYLLIUM UNDER THERMOMECHANICAL LOADING

PART 6: EFFECT OF PRESSURE ON THE MICROSTRUCTURE OF PLASMA-SPRAYED BERYLLIUM

Abstract

The effects of pressure and specimen preparation on the microstructure of two grades of porous plasma-sprayed beryllium were determined. One grade, P-1, was sintered after spraying while the other grade, P-10, was tested in the as-sprayed condition. The principal microstructural characteristics studied were grain size, grain morphology, and void distribution and size. It was found that machining can readily cause a significant dense surface layer on the porous beryllium specimens, and that the dense surface layer can be removed by etching. There was substantial difference in microstructure between the P-1 sintered and P-10 unsintered specimens both before and after being subjected to shock waves and static compression.

1. Introduction

This study is in support of an H-Division program on the computer simulation of the behavior of plasma-sprayed beryllium in shock environments. Knowledge and understanding of the beryllium microstructure is essential: (1) as basic input data to the computer models, (2) to insure that the beryllium used in laboratory tests is similar to that used in hardware, and (3) to insure that specimen preparation and experimental techniques do not alter the microstructure such that the modeling would apply only to those laboratory specimens. Following is a study of the microstructure of the plasma-sprayed beryllium used in the H-Division program. Several pertinent features and variations in microstructure, void shape and void distribution were found that would affect the modeling process and related codes.

This study can be considered in three broad categories:

- Initial microstructures.
- Effect of preparation.
- Effect of pressure.

INITIAL MICROSTRUCTURE

Two grades of beryllium were used, P-1 and P-10. Both grades are products of a single vendor, KBI.* The P-1 grade was sintered, while the P-10 grade was

*Reference to a company or product name does not imply approval or recommendation of the product by the University of California or the U.S. Energy Research and Development Administration to the exclusion of others that may be suitable.

Table 1. Index for photomicrographs showing initial plasma-sprayed beryllium microstructure.

		Figure	Magnification
Not sintered (P-10 Be)	Bright field	1	50X
		2a	400X
	Polarized	2b	400X
Sintered (P-1 Be)	Bright field	3	50X
		4a	400X
	Polarized	4b	400X

not. Table 1 relates the history of each specimen and the photomicrograph figure number. Magnitude, distribution and shape of the voids are most readily discerned in the 50X magnification bright field photomicrographs, while the beryllium microstructure and details of void shape may be examined in the 400X magnification bright field and polarized light photomicrographs.

Table 1 gives the photographic magnification and lighting information pertinent to the initial specimens shown in Figs. 1-4.

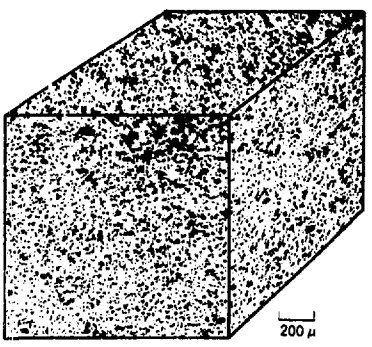

Fig. 1. P-10 beryllium, as-plasma-sprayed, not sintered. Top surface defined as transverse and side surface defined as longitudinal. Plasma spray direction perpendicular to top surface, ~50X, bright field.

EFFECT OF PREPARATION

The effect of machining, baking, etching, and epoxy coatings on microstructure and porosity was determined.

Table 2 outlines the histories of the specimens appearing in Figs. 5-11.

EFFECT OF PRESSURE

Three sets of experiments were carried out. The first two (10-kbar one-dimensional strain and 40-kbar hydrostat) were done by the Inorganic Materials Division,[1] and the third (shock-loaded utilizing a gas gun) by H Division.[2] The details of the pressurization experiments, discussed in Refs. 1 and 2, will not be repeated here. Table 3 summarizes the photographic results of all three experiments, giving photographic parameters and specimen numbers for Figs. 12-26.

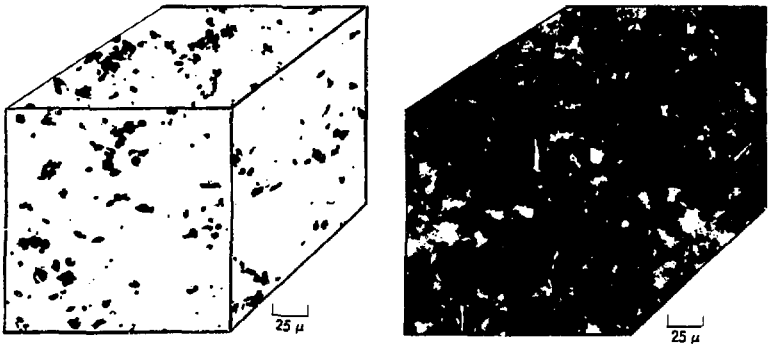

(a) Bright field (b) Polarized

Fig. 2. P-10 beryllium, as-plasma-sprayed, not sintered, ~400X, polarized.

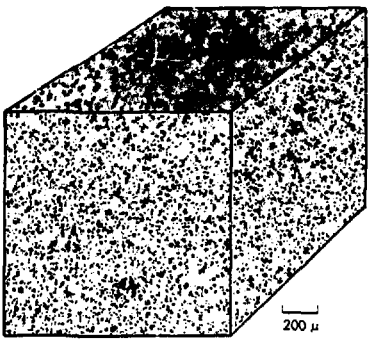

Fig. 3. P-1 beryllium, as-plasma-sprayed-and-sintered, ~50X, bright field.

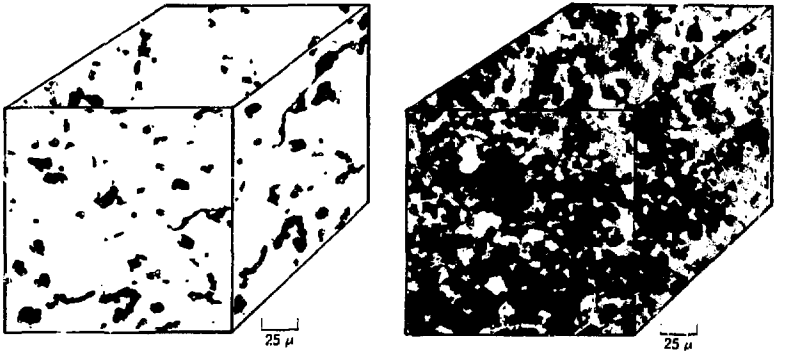

(a) Bright field (b) Polarized

Fig. 4. P-1 beryllium, as-plasma-sprayed-and-sintered, ~400X, polarized.

Table 2. Index for photomicrographs showing effects of specimen preparation.

		Machined		Baked (450°C)		Machined, baked (450°C), etched		Machined, baked (450°C), etched, epoxy coat	
		Fig.	Mag.	Fig.	Mag.	Fig.	Mag.	Fig.	Mag.
Not sintered (P-10 Be)	Bright field	5	400X	9a,b	400X	10a	400X		
	Polarized	6	400X						
Sintered (P-1 Be)	Bright field	7	400X	9c,d	400X	10b	400X		
	Polarized	8	400X					11	400X

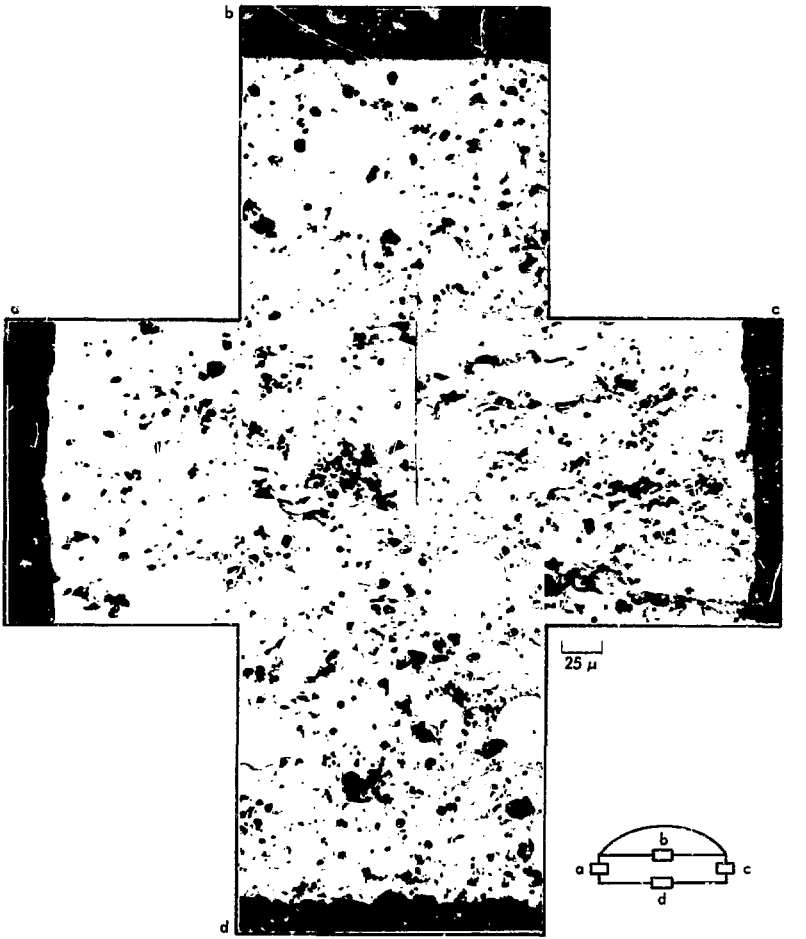

Fig. 5. P 10 beryllium, not sintered. Machined edges shown in (a), (b) and (c). As-plasma-sprayed edge in (d), ~400X, bright field.

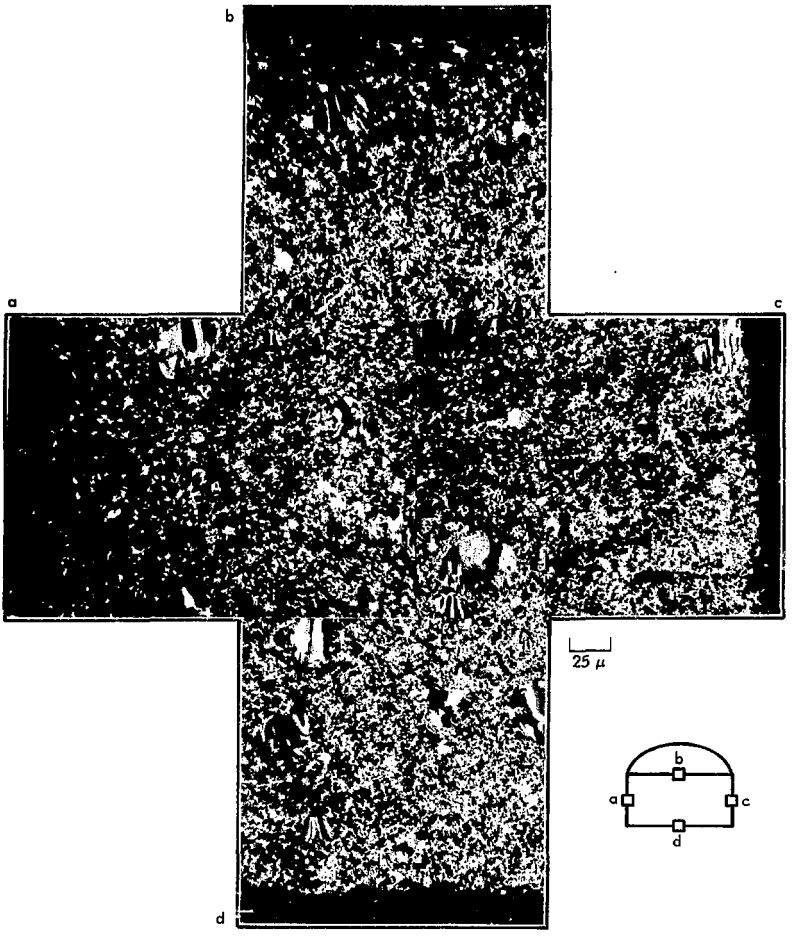

Fig. 6. P-10 beryllium, not sintered. Machined edges shown in (a), (b) and (c). As-plasma-sprayed edge in (d), ~400X, polarized.

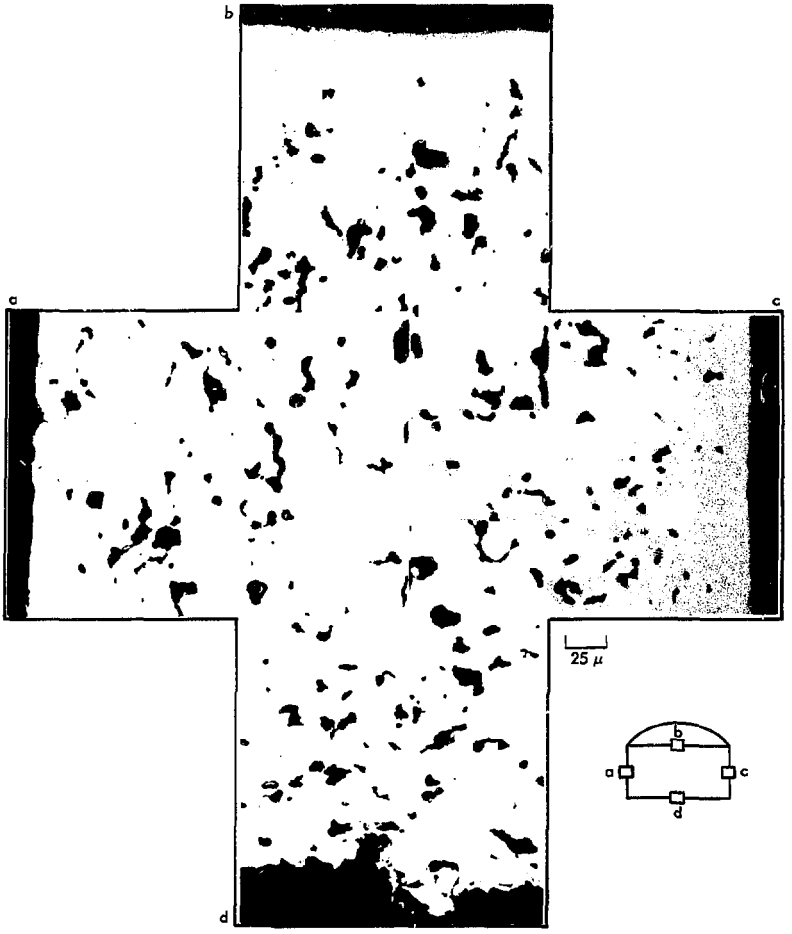

Fig. 7. P-1 beryllium, sintered. Machined edges shown in (a), (b) and (c). As-plasma-sprayed edge in (d), ~400X, bright field.

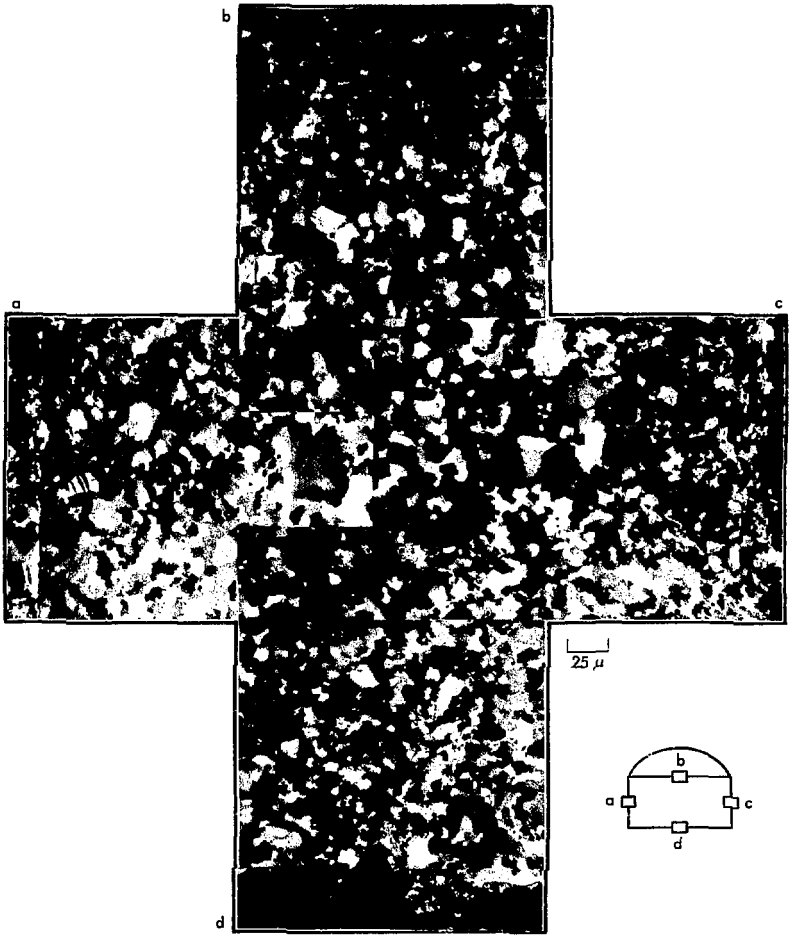

Fig. 8. P-1 beryllium, sintered. Machined edges shown in (a), (b) and (c). As-plasma-sprayed edge in (d), ~400×, polarized.

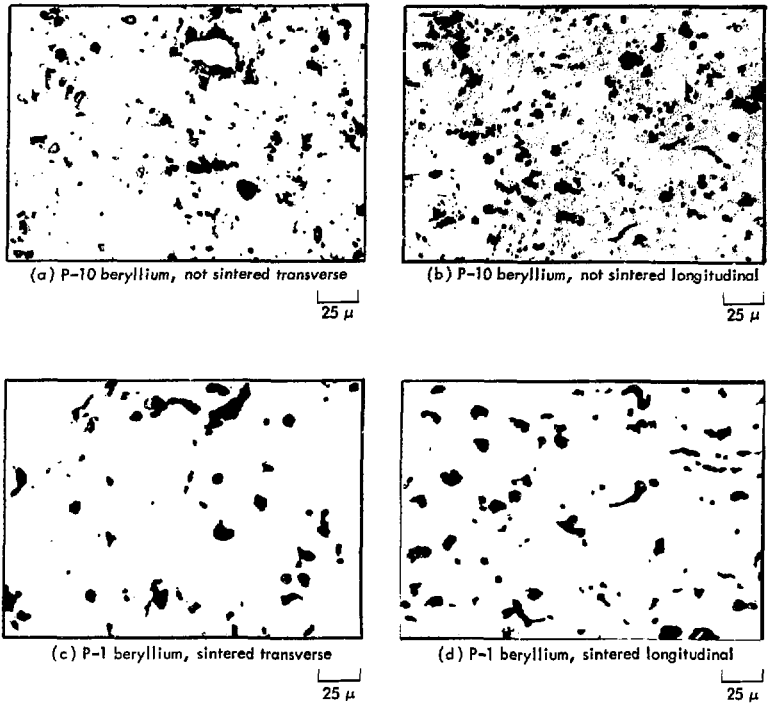

Fig. 9. Beryllium, plasma-sprayed and held at bake temperature of 450°C for 1 hr, ~400×, bright field.

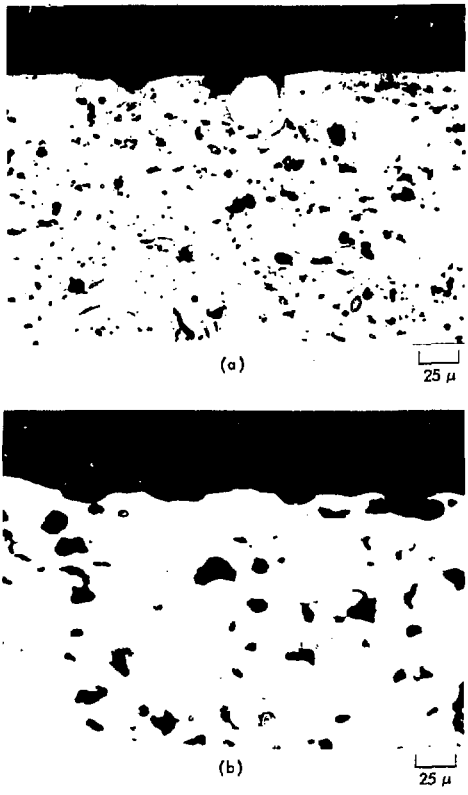

Fig. 10. Effect of etching machined surfaces, ~400X, bright field. (a) P-10 beryllium, plasma-sprayed, machined, baked and etched. (b) P-1 beryllium, plasma-sprayed, sintered, machined, baked and etched.

(a)

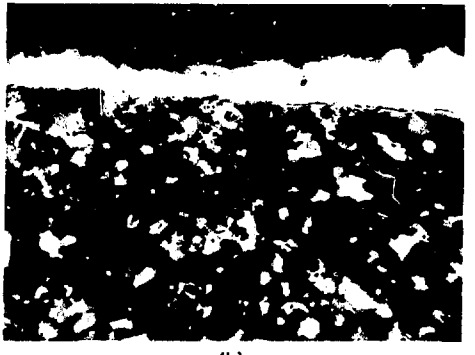

(b)

Fig. 11. Behavior of two epoxies on the surface of the plasma-sprayed-and-sintered beryllium, ~400X, polarized. (a) Hardman (gray layer) with Hysol (white layer) on the surface of beryllium. Layers of epoxy indicated by arrows. (b) Hysol layer (white) on surface of beryllium. Layer of epoxy indicated by arrow.

Table 3. Index for photomicrographs showing effects of pressure.

		10-kbar one-dimensional strain			40-kbar hydrostat			Shock-Loaded		
		Fig.	Mag.	Spec.	Fig.	Mag.	Spec.	Fig.	Mag.	Spec.
Not sintered (P-10 Be)	Bright field	12	50X	Be 2	16	50X	1			
		13a	400X	Be 2	18	400X	1			
					19	50X	2			
					20	50X	3			
	Polarized	13b	400X	Be 2	17	400X	1			
					18	400X	1			
Sintered (P-1 Be)	Bright field	14	50X	BeS1	21	50X	5	23	50X	BM
		15	400X	BeS1				24	400X	BM
								25	50X	BL
								26	400X	BL
	Polarized	15	400X	BeS1	22	400X	5			

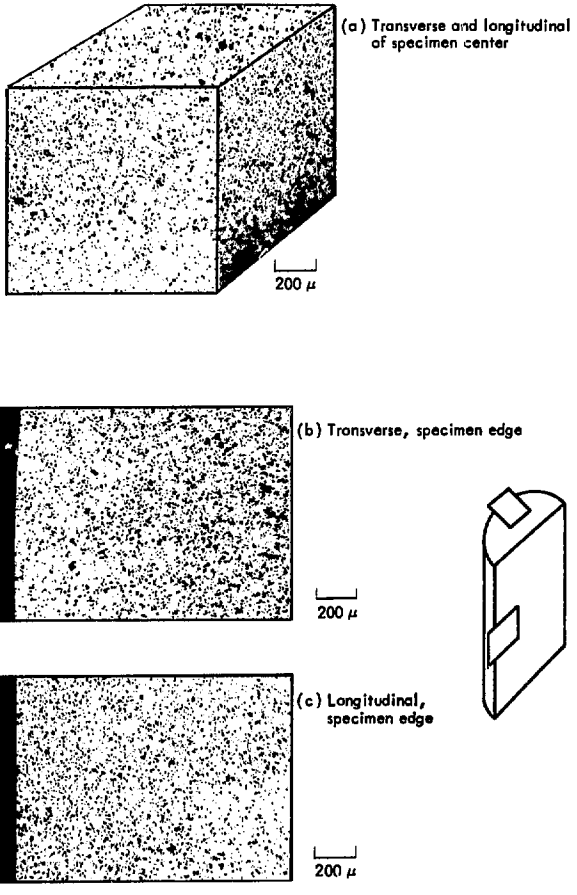

Fig. 12. P-10 beryllium, not sintered, 10-kbar one-dimensional strain. Specimen Be2, ~50X, bright field.

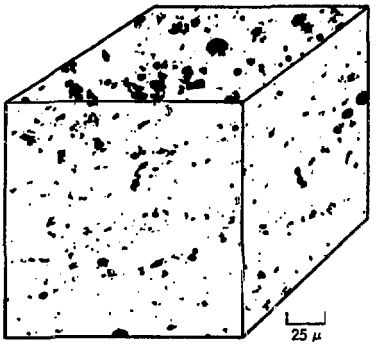

(a) Transverse and logitudinal of specimen center, bright field

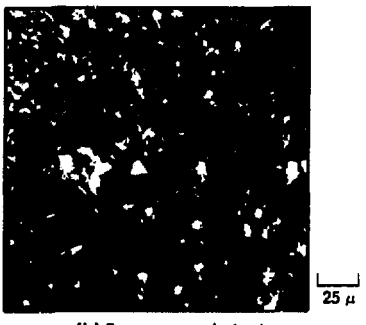

(b) Transverse, polarized

Fig. 13. P-10 beryllium, not sintered, 10-kbar one-dimensional strain. Specimen Be2, ~400X.

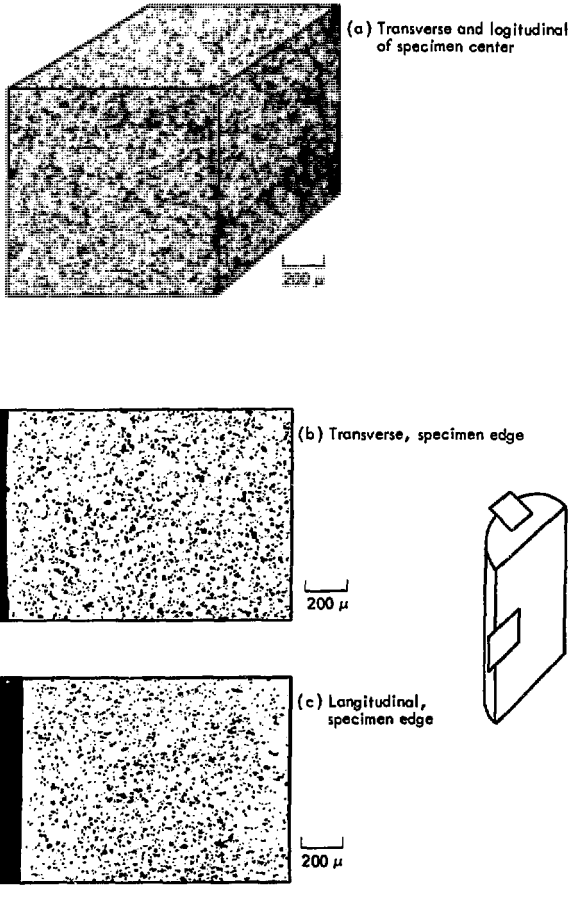

Fig. 14. F-1 beryllium, sintered, 10-kbar one-dimensional strain. Specimen BeS1, ~50×, bright field.

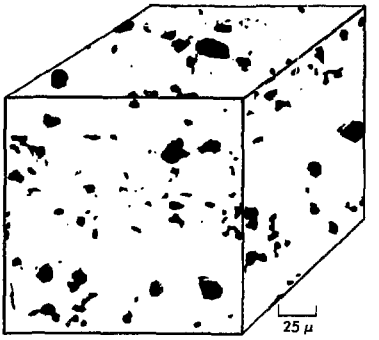

(a) Transverse and longitudinal of specimen center, bright field

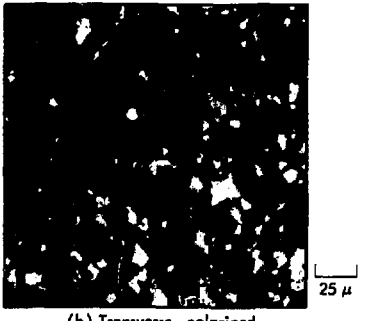

(b) Transverse, polarized

Fig. 15. P-1 beryllium, sintered, 10-kbar one-dimensional strain. Specimen BeS1, ~400X.

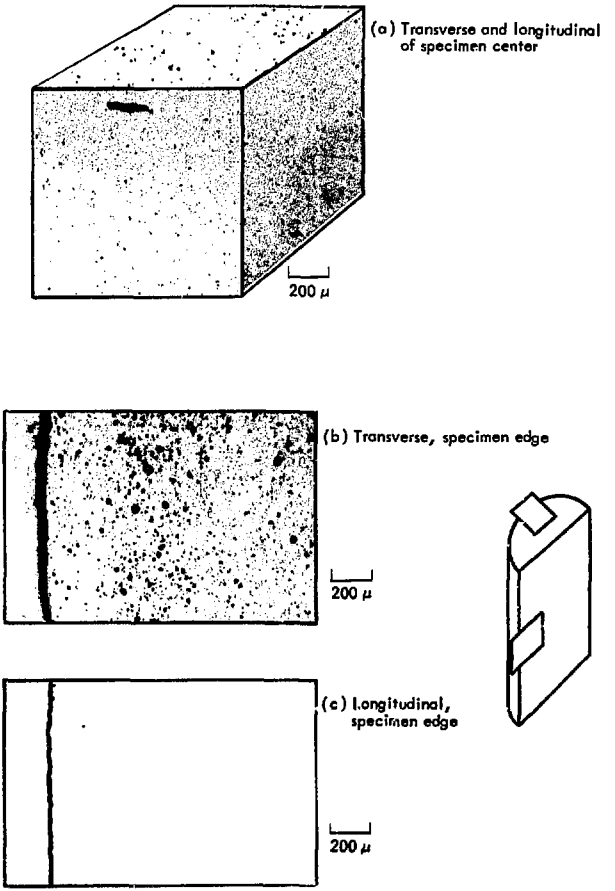

Fig. 16. P-10 beryllium, not sintered, 40-kbar hydrostat. Specimen 1, ~30×, bright field.

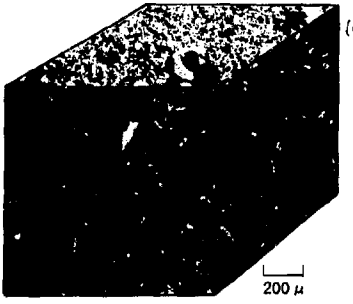

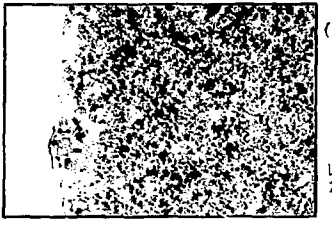

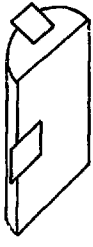

Fig. 17. P-10 beryllium, not sintered, 40-kbar hydrostat. Specimen 1, ~400X, polarized light.

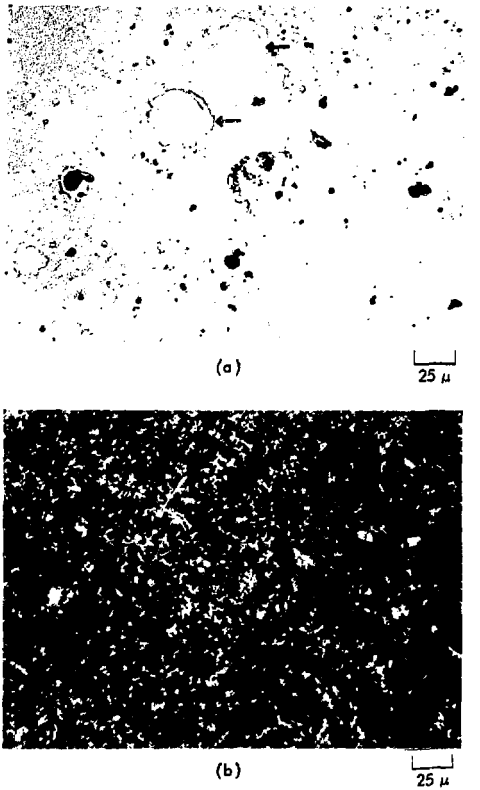

Fig. 18. P-10 beryllium, not sintered, 40-kbar, hydrostat. Transverse center cross section of Specimen 1. Arrows indicate typical void formation associated with colonies, ~400X. (a) Bright field, (b) polarized light, same area as (a).

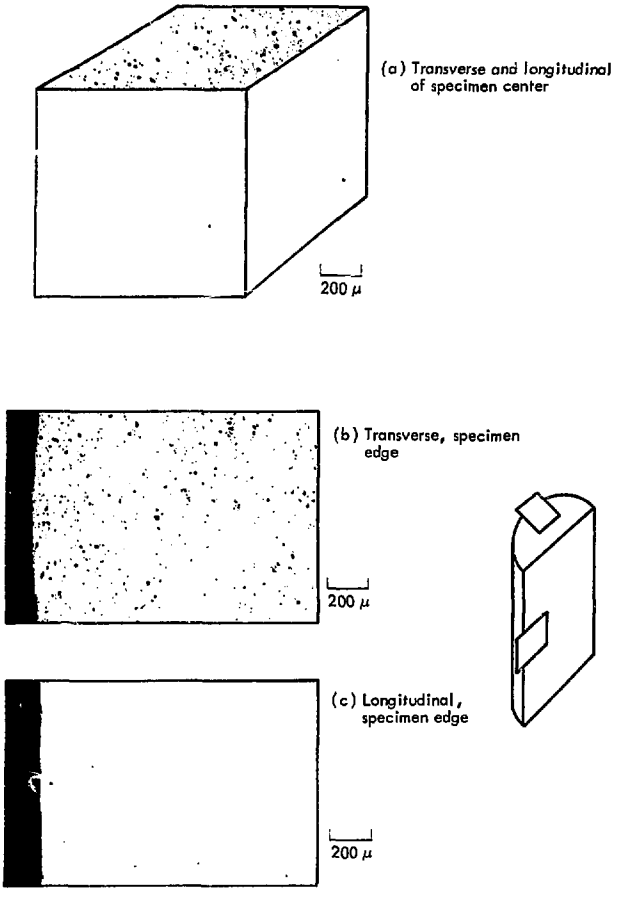

Fig. 19. P-10 beryllium, not sintered, 40-kbar hydrostat. Specimen 2, ~50X, bright field. (a) Transverse and longitudinal of specimen center. (b) Transverse, specimen edge. (c) Longitudinal, specimen edge.

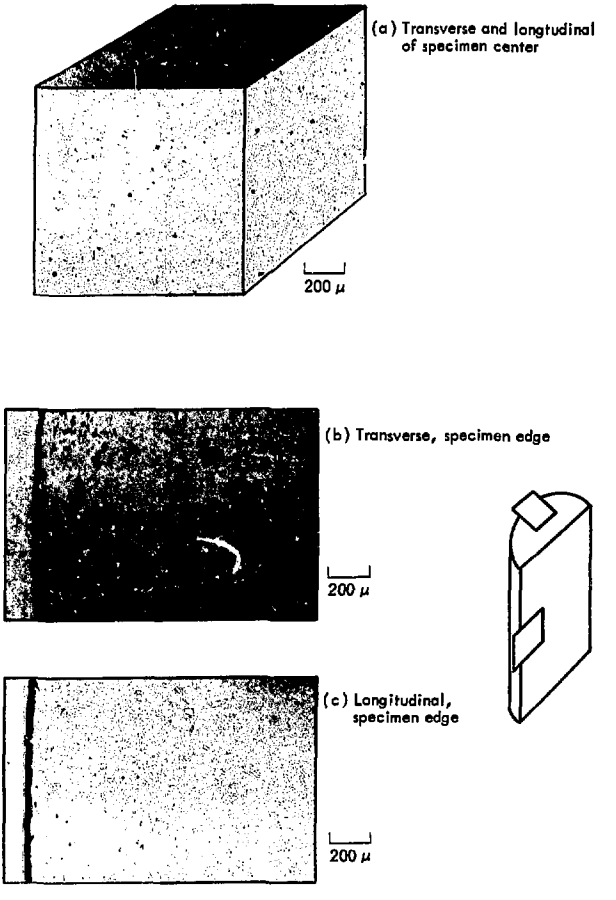

Fig. 20. P-10 beryllium, not sintered, 40-kbar hydrostat. Specimen 3, ~50X, bright field.

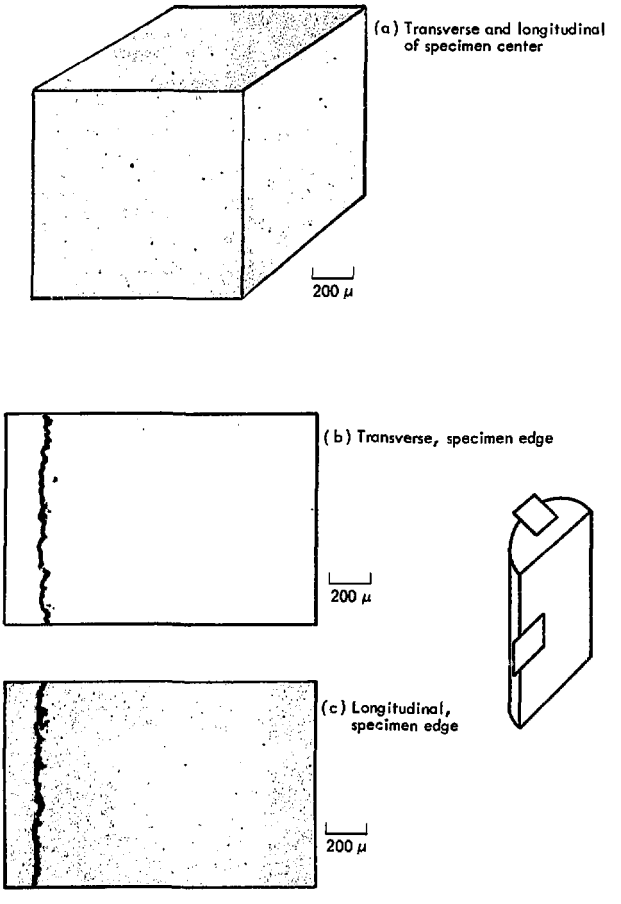

Fig. 21. P-1 beryllium, sintered, 40-kbar hydrostat. Specimen 5, ~50X, bright field.

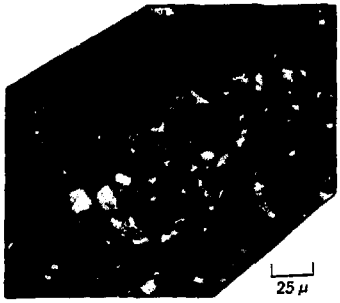

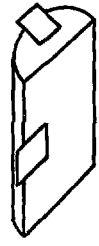

Fig. 22. P-1 beryllium, sintered, 40-kbar hydrostat. Specimen 5, ~400X, polarized light.

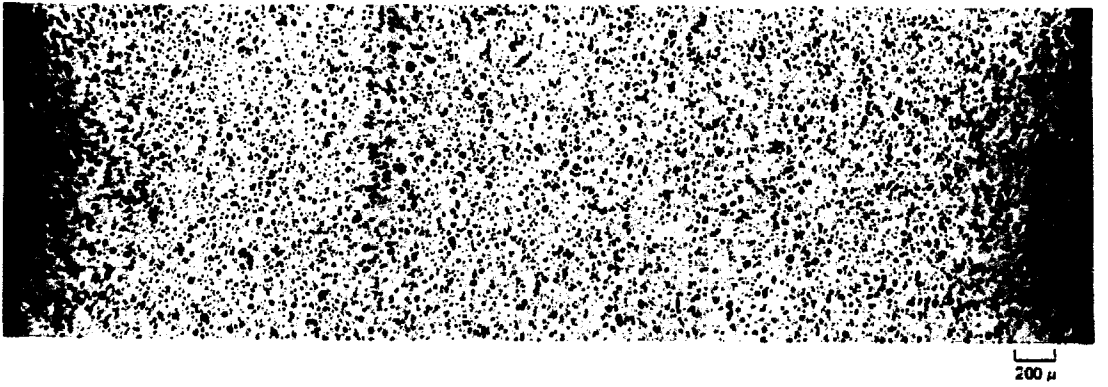

Fig. 23. P-1 beryllium, sintered and shock-loaded. Specimen BM, ~50X, bright field.

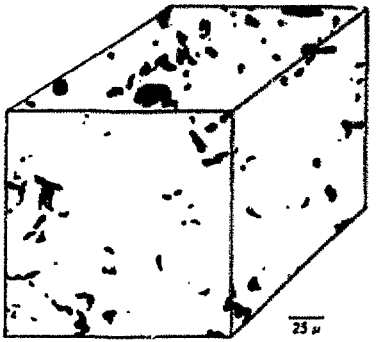

Fig. 24. P-1 beryllium, sintered and shock-loaded. Specimen BM, ~400X, bright field.

Fig. 25. P-1 beryllium, sintered and shock-loaded. Specimen BL, ~50X, bright field.

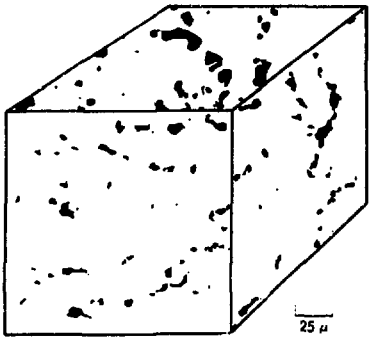

Fig. 26. P-1 beryllium, sintered and shock-loaded. Specimen BL, ~400X, bright field.

2. Material

Two grades of KBI beryllium were plasma-sprayed onto a 0.43-m-diam aluminum disk. Grade P-1 was sintered for 2 hours at 1175°C while Grade P-10 was not sintered.

Table 4 lists chemical impurity concentrations (supplied by the manufacturer) of the raw beryllium powder before spraying, and the densities of the original and compressed specimens.

Table 4. Chemistry and density of plasma-sprayed beryllliums P-10 and P-1.

		P-10 (-325 mesh, not sintered) (wt%)	P-1 (-325 mesh, sintered) (wt%)
Chemistry:	BeO	0.66	0.72
	Fe	0.075	0.035
	Al	0.024	0.006
	C	0.029	0.026
	Mg	0.026	0.002
	Si	0.010	0.008
Density:	Initial	88%	92%
	After 10-kbar one-dimensional strain	92%	96%

3. Results and Discussion

INITIAL MICROSTRUCTURE

As-Plasma-Sprayed P-10 Beryllium

Grain Structure—The as-plasma-sprayed microstructure of the P-10 beryllium is duplex. About 75-85% of the microstructure consists of grains 2 μ-in. diam or smaller, with the remainder consisting of 25-μ-size colonies containing 5-15 grains each (Fig. 2b).

Voids – The voids are irregular, but with a distinct disk-shape tendency. This can be observed by examining the shape of the individual pores (Fig. 2a); but it is more obvious by comparing the longitudinal and transverse sections (Figs. 1 and 2a). There are often void envelopes surrounding the large colonies. These envelopes can be observed in the as-plasma-sprayed microstructure (Figs. 2a and b) and specimens subjected to 40 kbar (Fig. 18). The shape of the void envelopes is considerably different than the other (disk-shaped) voids.

Sintered P-1 Beryllium

Grain Structure – The plasma-sprayed-and-sintered P-1 beryllium consists of a relatively uniform grain size of 8.3 μ (Fig. 4a). There are a few coarse grains of about 25-μ size that may be evolved from colonies similar to those found in the as-plasma-sprayed specimens.

Voids—The voids are more spherical in shape than those in the unsintered P-10 beryllium. This can be most easily observed by comparing the sintered longitudinal section to the sintered transverse section (Fig. 3) and to the unsintered longitudinal (Fig. 1) sections. The void envelopes associated with colonies in the plasma-sprayed condition were not observed in the plasma-sprayed-and-sintered P-1 beryllium.

SPECIMEN PREPARATION

Machining

There was no discernible effect of machining on the unsintered plasma-sprayed P-10 beryllium specimens (Figs. 5 and 6); there was, however, a pronounced effect on the sintered P-1 beryllium specimens (Figs. 7 and 8). In the P-1 specimens the machining caused a damage layer approximately 50-70 μ deep. It consists of: (1) a significantly lower void content than the bulk of the specimen, and (2) considerable twinning of the beryllium. The high-density layer is easily seen in Fig. 7a, b and c and it can be compared to the as-plasma-sprayed and sintered edge of the same specimen (Fig. 7d) and to the as-plasma-sprayed, unsintered and machined edges of the P-10 beryllium in Fig. 5a, b and c.

The twinning in the sintered specimens can be observed by polarized light (Fig. 8), and it extends to about the same depth as the low-void layer. Twinning damage at machined beryllium surfaces is common. Note the absence of twinning at the one surface that had not been machined (Fig. 8d). No evidence of twinning due to machining was observed in the unsintered P-10 beryllium specimen (Fig. 6); although the

very fine grain size could obscure a small degree of twinning.

It is possible that the higher purity, the coarser grain size, and the annealing process occurring during the sintering operation all contributed to a lower yield strength for the P-1 beryllium compared to the P-10 beryllium. This might enable more deformation to take place during machining with resultant void closure and a high-density layer at all machined surfaces. It is also possible that the P-1 specimen was machined more gently, i.e. had less material removed on the final machining passes, and thus showed no surface densification. It should be noted, however, that all the specimens tested in the shock wave and static compression studies were chemically etched deeply enough to remove any possible densified layer.

Bake

Grain Structure – The 450°C "baking" cycle to remove residual fluids after machining does not affect the microstructure. This was determined by optical microscopy (Fig. 9). There is a small possibility that some changes in the substructure may take place in the unsintered beryllium during the bake cycle. Transmission electron microscopy would be required in order to ascertain this. As it is unlikely that such low-temperature substructure changes would significantly affect the passage of shock waves, this possibility was not pursued.

Voids – There were no changes in the void morphology or distributions due to the bake cycle.

Etching

Following machining and baking, the plasma-sprayed specimens are etched. In Fig. 10 are typical cross sections at the machined edge of P-1 sintered and P-10 unsintered specimens. There is no high-density layer in either specimen; i.e., the etching procedure has removed the damaged layer in the sintered specimens. Thus etching is an essential step in specimen preparation to remove this potential source of anomalous behavior.

Strain Gage Mounting

In mounting the strain gages an epoxy with low viscosity (Hysol R8 -2038 resin and Hysol H2 -3490 hardener) is preferred for this application. To prevent the low-viscosity epoxy from penetrating the voids of the plasma beryllium and influencing the passage of the shock waves, the specimen had been coated first with a higher viscosity epoxy (Hardman Double/Bubble). In a recent experiment to determine the usefulness of this two-coat method, specimens were coated with appropriately dyed epoxies and cross sectioned. The photomicrographs (Fig. 11) show that neither epoxy penetrates significantly into the porous beryllium. Thus the simpler one-coat method can be employed without introducing anomalous high-density zones at the specimen surfaces.

EFFECT OF PRESSURE

10 kbar One-Dimensional-Strain Specimens

Grain Structure – No change in the grain morphology was observed after pressurization in either the P-1 sintered or P-10 unsintered specimen (Figs. 13 and 15).

Voids – The measured decrease in porosity upon pressurization is readily observed in the microstructure. In addition to the general decrease in porosity, there are several other changes which can be summarized as follows:

Shape – The porosity in both the P-1 sintered and P-10 unsintered specimens was disk-shaped with the thin dimension parallel to the axis. In the P-1 sintered specimen in which the voids had originally been somewhat spheriodized, this would be related to the higher axial pressure (about 10 kbar) compared to the radial pressure (about 5-6 kbar). In the P-10 unsintered specimen the porosity was initially disk-shaped from the plasma-spraying process. While the pressure most likely increased this tendency, it was not possible to discern this by optical micrography.

P-1 Sintered vs P-10 Unsintered – The size of individual voids in the P-1 sintered specimen is larger than that in the P-10 unsintered specimen (Fig. 12 vs 14). The total volume of porosity differs by up to 8%. This is difficult to judge, but it may be measured quantitatively by employing the appropriate automated techniques.

Edge vs Center – In the P-1 sintered specimen there is a substantial increase in density near the curved surface of the specimen. This zone of low porosity extends inward from the outside diameter about 0.05 mm, and it is observable in both the transverse and longitudinal sections (Fig. 14). Such a zone was not present in the P-10 unsintered specimen. Apart from 0.05-mm zone, in both the sintered and unsintered specimens there appeared to be some indication that the total volume of porosity gradually increased toward the center of the specimen.

40-kbar Hydrostat Specimens

Grain Structure – In the P-1 sintered specimens there is a small amount of twinning throughout the microstructure. This was not observed in the P-10 unsintered specimens, although the fine grain size in the latter specimens would obscure small amounts of twinning.

Voids – The voids surrounding the large colonies of grains noted in the as-plasma-sprayed P-10 specimens are still present in the specimens subjected to 40 kbar. Typical views of this phenomenon are shown in Fig. 18.

There are several unique features of the voids in the 40-kbar specimens:

Content – There is a dramatic decrease in void content in both the P-1 sintered and P-10 unsintered specimens (Figs. 16-22). In both the longitudinal and transverse cross sections of the P-1 sintered specimens and the longitudinal sections of the P-10 unsintered specimen, it is estimated that the void content is less than 1 to 2%.

Distribution – There is some tendency for the void content to be slightly less near the edges than in the center of the P-10 unsintered specimens (compare a, b and c in Figs. 16 and 20). However, this is not noticeable in a third P-10 unsintered specimen (Fig. 19) or in the P-1 sintered specimens (Fig. 21).

Shape – There is a substantial difference in void shape and distribution between the longitudinal and transverse cross sections of the P-10 unsintered specimens which does not exist in the P-1 sintered specimens. In the P-10

unsintered longitudinal specimens, the void content is low and the individual voids are small in size – similar to the longitudinal and transverse cross sections of the P-1 sintered specimen. However, in the transverse cross section of the P-10 unsintered specimen the void content appears to be considerably larger and the voids are relatively large and circular in shape. This was found in all three of the P-10 unsintered specimens that were examined (Figs. 16, 19, 20). A possible explanation of this peculiarity is that although voids have been flattened to the extent that opposite sides are essentially contiguous, they are not bonded and are easily separated. An elastic wave would most likely interact with this relatively large volume of flattened voids in the P-10 unsintered specimens, while such a condition does not exist in the P-1 sintered specimens.

Shock-Loaded Specimens

Two specimens that had been shock-loaded by H Division were examined. Specimen BM was impacted at 0.125 mm/μsec by a PMMA 1.87-mm impactor, and specimen BL was impacted at 0.289 mm/μsec by a PMMA 1.89-mm impactor. Both specimens had been sintered. The following observations were made:

- The general pattern and shape of the voids were similar to that of the 10-kbar one-dimensional-strain specimens. The voids in both the BM and BL specimens were disk-shaped and, qualitatively, the total void content appeared to be very slightly less and the voids somewhat flatter than the 10-kbar one-dimensional-strain specimens. However, they did not approach the high density achieved in the 40-kbar hydrostat specimens.
- There is no increase in density at the edges of the shock-loaded specimens. At both ends of the BL specimen, the density is higher and the voids flatter than in the bulk of the specimen. This was not observed in the BM specimen.

OTHER VARIABLES

Two material characteristics of the plasma-sprayed beryllium – texture and grade of input beryllium powder – have not been considered here, but will influence the passage of a shock wave.

It is known that the characteristics of a shock wave passing through beryllium depend on the crystallographic direction. It has been shown that in high-purity single crystals the Hugoniot elastic limit is highest when the direction of the wave is such that the pyramidal slip systems are activated, intermediate when prism slip systems are activated, and lowest when the basal slip system is activated. A clearly defined elastic precursor with a risetime in the low-nsec region is observed for each of the three slip systems.[3] For a polycrystalline beryllium specimen in which there is little crystallographic texture (such as hot-pressed block), no clearly defined elastic precursor exists and the risetime is in the range of a few hundred nsec.[4] However, if a polycrystalline beryllium specimen has a crystallographic texture, there is a definite elastic precursor wave. The risetime is in the few-nsec range, similar to that for the single crystal, and it decreases with increasing degrees of texture.

Two different grades of beryllium were employed, viz., P-1 and P-10; the P-1

beryllium is the purest. The higher purity usually results in higher elongation and lower ultimate and yield strengths, although the strengths can be greatly enhanced by special processing techniques. The possible difference in the strength of the two materials can be illustrated by considering the properties of the two powders hot-pressed under approximately similar conditions:

	Ultimate strength MPa(ksi)	Yield strength MPa(ksi)	Elongation (%)
P-10	420 (61)	289 (42)	4-9
P-1	400-558 (58-81)	265-372 (38-54)	6.0-7.3

While these specific values would not apply quantitatively to the plasma-sprayed material, the large difference in strength and ductility are indicative of the inherent differences of the two materials. It is interesting to note that the sintering characteristics of the high-purity P-1 beryllium differ from those of the low-purity P-10 beryllium. This will result in differently shaped voids in the two materials with the same sintered density; and there is evidence that the differently shaped voids cause different mechanical properties. Other factors being equal, the yield strength of beryllium increases with decreasing grain size, and the grain size of the two materials here varies by a factor of four. Thus, in addition to the differences in densities of the two materials, there are several other differences between the two materials that affect their mechanical behavior.

4. Summary

The microstructure of the as-plasma-sprayed P-10 beryllium is duplex with a preponderance of 2-μ-size grains and the balance consisting of 25-μ-size colonies of about 10 grains. The voids in the P-10 beryllium are mainly irregularly shaped disks, although another type of void tends to partially envelop the 25-μ-size colonies. The sintered P-1 beryllium microstructure consists of uniform equiaxed grains about 8 μ in size, and the voids tend to be relatively spherical in shape.

The machining operation caused a significant collapse of pores and an attendant high-density surface layer. The high-density layer could be removed by chemical etching and, indeed, this was done for all specimens in the program.

The principal effect of the 10-kbar one-dimensional strain and the shock loading on both types of plasma-sprayed beryllium was a decrease in void volume, and a tendency for the voids to become more disk-like in shape. The void content of the 40-kbar hydrostat specimens is very small in both the P-1 and P-10 beryllium. The void shape in the P-1 40-kbar hydrostat specimens is similar in the longitudinal and transverse directions. In the P-10 unsintered specimens the void shape and distribution differs with orientation. The voids in the longitudinal cross section are small and disk shaped – similar to those of the P-1 sintered specimen; and the voids in the transverse cross section are relatively large and more circular in shape.

Acknowledgments

The authors are grateful to W. M. Isbell, R. R. Horning, R. N. Schock, A. E. Abey, and A. G. Duba for providing the beryllium specimens and background information.

References

1. R. N. Schock, A. E. Abey, and A. G. Duba, Behavior of Porous Beryllium Under Thermomechanical Loading: Part 2. Quasi-Static Deformation, Lawrence Livermore Laboratory, Rept. UCRL-51682-2 (1974).
2. W. M. Isbell and R. R. Horning, Behavior of Porous Beryllium Under Thermomechanical Loading: Part 3. Shock Wave Studies, Lawrence Livermore Laboratory, Rept. UCRL-51682-3 (1974).
3. L. E. Pope and A. L. Stevens, "Wave Propagation in Beryllium Single Crystals," Metallurgical Effects of High Strain Rates, AIME 1973 Conf. (Plenum Press, 1973) p. 349.
4. A. L. Stevens and L. E. Pope, "Wave Propagation and Spallation in Textured Beryllium," Metallurgical Effects of High Strain Rates, AIME 1973 Conf. (Plenum Press, 1973) p. 459.

RBC/edas/lmc